

Parasitic Effects in Impedance Spectrum of PEM Water Electrolysis Cells: Case Study of High-Frequency Inductive Effects

Irene Franzetti,* Artem Pushkarev, Ai-Lin Chan, and Tom Smolinka

Electrochemical impedance spectroscopy (EIS) is a powerful tool to characterize and distinguish electrochemical, electrical, and diffusive processes in an electrolysis cell. The EIS response with small impedance ($m\Omega$) depends on components and materials of the cell, but often also on the electrical setup, cables, and connectors, leading to incorrect conclusions about the performance of the electrolysis cells. These parasitic effects are assessed via a short-circuit measurement and confirmed to be external from the membrane electrode assembly (MEA). In the setup, the inductive characteristic is described by a modified inductive reactance and must be included in the equivalent circuit model (ECM) which is fitting the cell EIS spectra in operation (in situ). If points of the spectra showing inductive characteristic (below x -axis in Nyquist plot) are excluded from the ECM evaluation, an artificially increased ohmic resistance at high frequencies is obtained. In addition, considerations on other components of the ECM can be misleading and significantly incorrect. The only way to avoid that inductive behavior caused by the external setup is incorrectly assigned to the ECM describing properties of the MEA is to include the inductive effects in the ECM analysis of in situ EIS measurements.

1. Introduction

Electrochemical impedance spectroscopy (EIS) is an important noninvasive method to monitor the performance of an electrochemical cell, such as batteries, fuel cells, and electrolysis cells.^[1–8] With this widely used and powerful characterization method, it is possible to distinguish electrochemical and electrical processes in the cell based on their frequency response. When this technique is backed up by an equivalent circuit model (ECM) analysis, the evaluation of the addressed electrochemical process, interfacial contacts, proton migration, and water or gasses diffusion is enhanced. Via an ECM, in fact, it is possible to conceive these internal processes as electronical elements, such as capacitances and resistances. The prerequisite for conceiving an ECM is, therefore, the knowledge or assumption of the expected processes to be happening during cell operation. Further considerations are going to be explained in Section 2.4.

It is mentioned by Cruz-Manzo et al. and before also by Savova-Stoynov et al. that the response of a cell with low impedance ($<1\ \Omega$) does not only depend on its components and materials, but it is often influenced by external parasitic effects. The latter may come from the setup of measurement instruments in the form of inductivities.^[4,9] Especially for higher current densities, these effects can become significant and affect the shape of the impedance spectra, and hence its evaluation.^[4,9,10]


In case of impedance spectra for electrolysis cells, an inductance is an unwanted effect attributable to a time-varying magnetic field caused by an AC current. This varying magnetic field can change the inductance and resistance of the cable that carries the AC current, as well as of nearby cables in the setup. The former case causes a so-called self-inductance and an increased resistance, related to the skin effect. The latter creates a mutual inductance on the adjacent cables and an increased resistance explained by the proximity effect. If sense cables are affected by the AC current of the current-carrying cables, a variation in the measured voltage is induced.

An inductive reactance (Z_L) in an impedance spectrum appears as points in the positive imaginary part of the Nyquist plot. It has positive phase angle ($\varphi = 90^\circ$) and it is directly dependent on the frequency f , per Equation (1).^[4,9]

I. Franzetti, A. Pushkarev, T. Smolinka
Chemical Energy Storage
Fraunhofer Institute for Solar Energy System ISE
Heidenhofstrasse 2, D-79110 Freiburg, Germany
E-mail: irene.franzetti@ise.fraunhofer.de

A. Pushkarev
HySA Infrastructure Center of Competence
Faculty of Engineering
North-West University
Private Bag X6001, Potchefstroom Campus, 2531, South Africa

A.-L. Chan
Chemical and Material Sciences Center
National Renewable Energy Laboratory
15013 Denver West Parkway, Golden, CO 80401, USA

 The ORCID identification number(s) for the author(s) of this article can be found under <https://doi.org/10.1002/ente.202300375>.

© 2023 The Authors. Energy Technology published by Wiley-VCH GmbH. This is an open access article under the terms of the Creative Commons Attribution License, which permits use, distribution and reproduction in any medium, provided the original work is properly cited.

DOI: 10.1002/ente.202300375

$$Z_L = j|Z|\sin\varphi = j\omega L = j2\pi fL \quad (1)$$

The corresponding inductance L is independent from the frequency. For measurements on proton exchange membrane (PEM) electrolyzer, all points of this positive imaginary part of the impedance spectrum is usually ignored by ignoring the spectrum points below the x -axis.^[11,12] However, this might lead to significant overestimation of the high-frequency resistance (HFR) of the electrochemical cell. As suggested for a solid-oxide electrolysis cell by Shin et al., this inductance may shift the spectra to higher positive impedances.^[13] Therefore, these parasitic effects need to be taken into account in an ECM to interpret the obtained EIS results correctly.^[4] For instance, the practice of using the intersection of the impedance spectrum with the x -axis as the so-called HFR value to estimate the Ohmic resistance of the PEM fuel cell (PEMFC) might lead to large errors (10–50%).^[14] The error extent depends on the frequency range used and the magnitude of the inductance. According to Cruz-Manzo et al. for a 25 cm² PEMFC, the value of the inductor $L = 2.07 \times 10^{-10}$ H was considered negligible. But when stronger inductor component exists, it has to be considered in ECM modeling.^[15]

Klotz and Shin reported that in the high-frequency range (>1 kHz) certain inaccuracies may occur due to the wiring inductivities.^[13,16] Similar effects coming from the instrument setup (potentiostat/power supply internal components, i.e., cables, voltage, and current amplifiers) were also discussed by Erinmwingbovo et al., in a study on instrument artifacts on EIS.^[17] Other studies have reported that it is necessary to optimize the length, position, and type of cables, and the electrical connections of the measurement system to reduce interference signals. Inductance artifacts from the experimental setup could be reduced by maintaining equal and shortest length of the cables, using a four-point circuit, twisting and shielding the large current cables, and polishing and clamping the metal contacts.^[4,9,18–20] In addition, according to the study of Asghari et al., an inductive behavior of PEMFC at high frequencies resulted from a nonuniform contact (assembly) pressure.^[19] Inductance was gradually diminished as the level of uniformity of the assembly pressure has been increased.

The inclusion of parasitic effects within the evaluation of the whole cell spectra has already occasionally been done in other studies on PEM^[5,21] and alkaline^[22] electrolysis cells. A validation methodology to assess external influences on the impedance spectra of a solid-oxide fuel cell (SOFC) was suggested by Raikova et al., who observed the influence on the high-frequency part of the spectra, as well as on the polarization resistance, and therefore, at low frequencies.^[23] They subtracted the impedance measured in a short-circuit (SC) test from the operating impedance of the SOFC assuming it as additive to the impedance of the object. This approach can be constrictive, in case for example that the test measures interfacial resistances of components that are influencing the performance of the SOFC. They also considered this external impedance a pure inductance and subtracted as such, even if they evidenced a deviation from this behavior.

While parasitic effects have been addressed in different electrochemical setups and with different approaches, a more stringent methodology to assess these external influences is lacking. In addition, a study quantifying the effects of not including these

parasitic effects in the ECM evaluation of a PEM water electrolysis cell is void, so far. Thus, this study describes and discusses a methodology (SC measurement) to assess external influences, and how to use the modeled parasitic effect as basis for the ECM analysis on the in situ EIS measurements. In addition to this, it is examined how excluding the points of the spectra with inductive characteristic can influence the parameters of an ECM and lead to misleading evaluations.

2. Experimental Section

2.1. Test Setup, Cell, and Hardware

From now on, the measurement used for assessing the external influence is going to be referred as SC measurement, while the in situ measurement is the test done with an actual PEM water electrolysis cell. The in situ and SC measurements were performed with a single test cell in a self-constructed test bench provided with two separated water circulation loops for anode and cathode. The loops were provided with gas water separators, pumps, and ion exchangers. One single heat exchanger heated up both loops to the required temperature of 80 °C thanks to a Julabo cryostat CF31. The testbench was automatically controlled via LabVIEW and the electronics used were a potentiostat (Zennium PRO, Zahner-Elektrok GmbH), a load (EL1000, Zahner-Elektrok GmbH) which sank the current provided by a power source SM18-220 from Delta Elektronika. The electrical connection to the cell was achieved via twisted and shielded current collector cables, as well as twisted and shielded voltage sense cables. Each cable was kept as short as possible, and voltage and current cables were connected at the same point of the anode and cathode current collectors, providing a 2-point connection to the cell.

The cell used was presented in a previous doctoral thesis.^[24] Its reduced (without endplates and clamping system) drawing is shown in **Figure 1** with its corresponding ECM, which is more thoroughly explained in Section 2.4. The cell consisted of

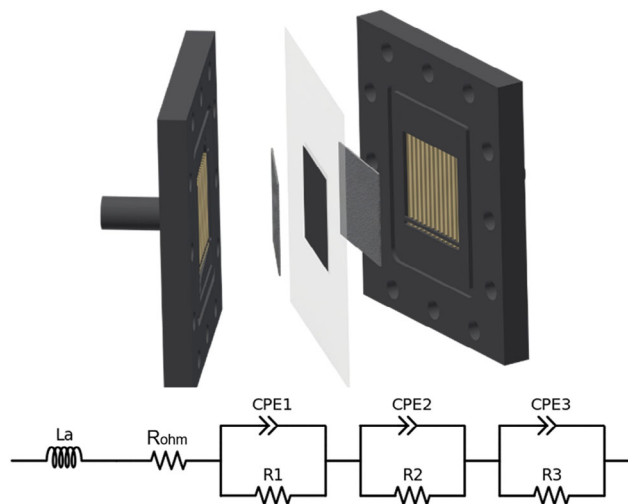


Figure 1. Schematic cell setup used for in-situ measurement and the corresponding equivalent circuit model (ECM).

titanium end plates with gold-coated flow field structure inserted in an isolating frame. The current-carrying cables and voltage senses were connected to these end plates. Two 1 mm thick porous transport layers (PTLs) consisting of sintered titanium fibers (2GDL40 Bekaert) were used. The PTLs were sputtered with Ir and IrOx coatings and placed on the flow fields of cathode and anode side respectively. The catalyst-coated membrane (CCM) inserted between the PTLs had an active area of 23 cm^2 and was provided with 2.3 mg cm^{-2} IrOx catalyst layer on the anode side, 0.35 mg cm^{-2} of Pt supported with carbon on the cathode side, and a $120 \mu\text{m}$ thick perfluorosulfonic acid membrane (Fumasep) produced by Fumatech BWT GmbH.

2.2. In Situ Protocol, Polarization Curve and EIS

The activation and conditioning protocol of the CCM was conducted at $80 \text{ }^\circ\text{C}$, ambient pressure, and a supplied water flow rate of 0.2 L min^{-1} on both cathode and anode sides. The CCM was activated via two galvanostatic steps at 0.2 and 1 A cm^{-2} for half an hour each. This first step was followed by a potentiostatic step at 2.2 V held for 10 h. Subsequently, three galvanostatically driven polarization curves from 0.01 up to 4.5 A cm^{-2} and back down to 0.01 A cm^{-2} were performed. The potentiostatic step and the polarization curves were repeated two more times. At last, another potentiostatic held at 2.2 V for 10 h step was carried out and the beginning of life characterization of the cell was conducted via three additional polarization curves and EIS.

Here, we would only report the EIS results of the last polarization curve of the explained conditioning protocol (in situ measurements) and compare them with the EIS results from the SC measurements (see Section 2.3), which were performed without a CCM in the test cell. EIS measurements were performed during SC and in situ measurements at the current densities of 0.3 , 1.0 , 2.0 , and 3.0 A cm^{-2} . The spectra were recorded for frequencies ranging between 0.1 Hz and 10 kHz . The collected points per decades were 20 for frequencies higher than 60 Hz , and 10 points per decades for lower frequencies. The number of averaged cycles was selected to 5. Before each EIS measurement, the chosen current density was held for 3 min to have a stable temperature and voltage response and the amplitude of the AC signal was set to 5% of the DC current input. All in situ results reported in this work were based on mean values of three identical tests from three fresh CCMs of the same production batch which were activated as described earlier.

2.3. SC Measurements

The testing setup of the SC measurements required the cell to be connected electronically and physically to the testbench used in the in situ measurements. The assembled cell is sketched in **Figure 2**. It was the same one used for in situ measurements, provided with all components, but instead of the CCM, a 0.25 mm thick gold-coated titanium plate was placed in between the two PTLs of the cell.

With this setup, all contributions of the hardware used for in situ measurements except from those originating from the CCM itself could be obtained. The assembled cell was, in fact, tested

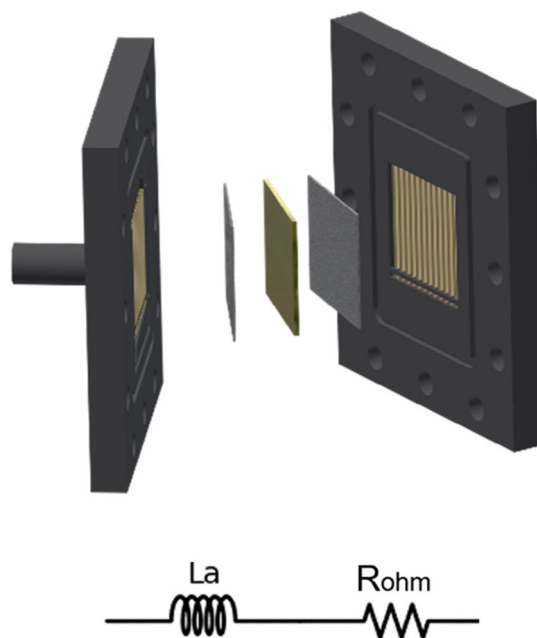


Figure 2. Schematic cell setup used in short-circuit measurement and the corresponding ECM.

under different current densities via EIS, as explained in Section 2.2. The results were then evaluated via the fitting model below the schematics of the cell.

2.4. ECM

A fitting model of an EIS spectrum was an electrical circuit called ECM and it was used to illustrate and account for the phenomena representing the electrochemical response of the cell. To fit the EIS spectra of a fuel cell or an electrolysis cell, many models were suggested by the scientific community, but a general ECM has not yet been employed by the majority, since in the different works different issues and materials were investigated. Fitting models used for electrochemical hydrogen cells varied a lot in different approaches: the most typical model was the basic Randle cell,^[25] where effects due to electrical and protonic movements were fitted by a resistance, in series with a parallel group composed of a resistance (the charge-transfer resistance) and a capacitance (the double-layer capacitance), both belonging to effects at the catalyst layer.^[6] Transmission line models were preferred when the focus was on the catalyst layer behavior.^[25,26] A capacitance was substituted by a constant phase element (CPE) in case the inhomogeneities of the porous catalyst layers wanted to be included. Effects related to mass transport limitation could be addressed by including a Warburg element (Wrb) in the parallel group or by an additional group of resistance in parallel with a capacitance (R//C).^[5,19,27] Depending on the materials analyzed and the operating conditions, the EIS spectra might include one, two, or three resistance and capacitances in parallel (R//C groups), to assess effects at high, medium, and low frequencies.^[19]

Rozain and Millet considered the EIS spectra as results of two processes (two R//C) coming from the anode side, with

negligible influence of the cathode part.^[28] The same approach has been proposed by Siracusano et al., but the parameters of R//CPE at high frequencies appeared to be sensitive to cathode catalyst loading.^[6] The chosen ECM was composed by an Ohmic resistance (R_{ohm}) and two R//CPE groups. Rozain et al., in a subsequent paper, used the same ECM and attributed the two R//CPE characteristics to anode and cathode, to easily assess the anode catalyst layer, which was the focus of their paper.^[29] Rasten et al. also used the same ECM and suggested the mechanisms as two steps of the oxygen evolution reaction, via comparing EIS of cells with different annealing temperatures of the anode catalyst powder.^[30]

Van der Merwe et al. used an ECM composed by an inductance (L) in series with R_{ohm} and with one (R_{ct} -Wrb)//CPE group, to have three elements, which could be associated to the losses in the polarization curve. The selection of this model was supported by the analysis of the polarization curves slope and of the Tafel slope, as comparison parameters to the R_{ohm} and R_{ct} //CPE groups, respectively.^[5]

An ECM with an R_{ohm} and three R//CPE groups was used to fit the EIS of a PEM electrolysis cell measured by Elsoe et al.^[8] Since the EIS at high current densities were showing three arcs, the processes were decided to be modeled by 3R//CPE groups.^[8] The high-frequency arc was assumed to be related to limitations at the triple-phase boundary, as electrolyte–electrode restrictions, while the other two arcs were associated with two distinguished mechanisms at the anode catalyst layer. The same model with an additional L was also used by Lettenmeier et al., to fit EIS from a cell with and without a microporous layer.^[31]

Before applying any fitting to the collected data, the linearity, causality, and time invariance dependence of the data were evaluated via Kramers–Kronig test (KKT) and the inconsistent data points were excluded.^[4,5,32] All the measured points showed reliable and performing EIS response according to KKT and these results were not reported in this paper, since they were not the focus.

In literature as well as in this study, much attention it is given to the characteristics of the Bode and Nyquist plots, since their shape could give an indication of the electrochemical effects and the corresponding elements composing the ECM. To evaluate the EIS results of the SC measurement, an ECM composed by an R_{ohm} and a modified inductive reactance (L_α) in series was used (Figure 2). The impedance resulting from L_α described inductive effects heterogeneously distributed to the frequency f and dependent to a coefficient α . When α was 1, L_α described the reactance of a pure inductance, similar to the behavior of a CPE for a distributed capacitor, where $\alpha = 1$ described a pure capacitor. The impedance of this modified inductive reactance was defined by Equation (2).

$$L_\alpha = L(j2\pi f)^\alpha \quad (2)$$

For the in situ measurements, L_α , R_{ohm} , and three groups with a resistance in parallel with a CPE (R//CPE) were used (Figure 1). This has proven necessary to be able to use one single model for multiple current densities. Two arcs were seen at current densities below 3 A cm^{-2} , and therefore, two processes were underlying in these ranges and could be modeled via two R//CPE groups. However, with increasing current densities, an

additional arc appeared at very low frequencies. This could be due to mass transport limitation, for instance, due to the limited access of reactant water because of bubble formation, and could be fitted via a third R//CPE group.^[33] The CPE were characterized by an equivalent capacitance (C) defined as^[34]

$$C = Q(\omega_{max}'')^{n-1} \quad (3)$$

where ω_{max}'' is the frequency where the imaginary impedance has its maximum. A time constant (τ) was calculated from the equivalent capacitance and the charge-transfer resistance R_{ct} in parallel to the CPE as

$$\tau = CR_{ct} \quad (4)$$

From the τ , the peak frequency (f_{peak}) could be evaluated per

$$f_{peak} = \frac{1}{2\pi\tau} \quad (5)$$

The model was executed via an in-house written Python code using a specific package called impedance.py.^[35] The recursive iteration to reach the best fit needed as input parameters: 1) the ECM, 2) initial values of each element, and 3) their ranges. The accuracy of fit was evaluated via the parameter χ^2 .^[27,35]

3. Results and Discussion

3.1. SC Measurements and ECM Fitting

The EIS results during SC measurement at each of the four applied current densities show a slightly noisy response. The data points are, therefore, filtered to reduce the noise and the filtered results are depicted in **Figure 3**. The EIS response shows similar spectra for current densities above 1 A cm^{-2} . The threshold between 0.3 and 1 A cm^{-2} corresponds to the switch between shunts internal to the potentiostat, which is believed to be origin for the slight difference between spectra. However, this difference is very small ($1 \text{ m}\Omega \text{ cm}^2$), considering the accuracy of the device, and could not be reduced any further. The latter is attributable to the specifications of the potentiostat and its lower accuracy at lower current densities. Overall, the SC measurements show a real-only impedance behavior of around $19.5 \text{ m}\Omega \text{ cm}^2$ up to 60 Hz , but, above this frequency, a higher absolute impedance up to $45 \text{ m}\Omega \text{ cm}^2$ dominates the response. This is evident in the Bode plot of **Figure 3b**, as well as in the increasing phase angle in the Bode plot of **Figure 3c**.

The common ECM used for the SC measurements, with its pure electrically conductive components and the interfaces between them, would be a simple resistor (model R in **Figure 3**). However, the results evidence an additional and simultaneous effect to the supposed resistive behavior: its positive phase angle and increased impedance with increasing frequency (**Figure 3b**). This is generally the behavior of an inductor L , according to Equation (1).

The results prove that the external setup, instead of the membrane electrode assembly (MEA), is responsible for this additional effect. Many attempts to avoid any parasitic effect have been performed: the instruments are calibrated, the wiring is shielded and twisted to the maximum extent possible, and the current-carrying cables are shielded and kept as short as possible.

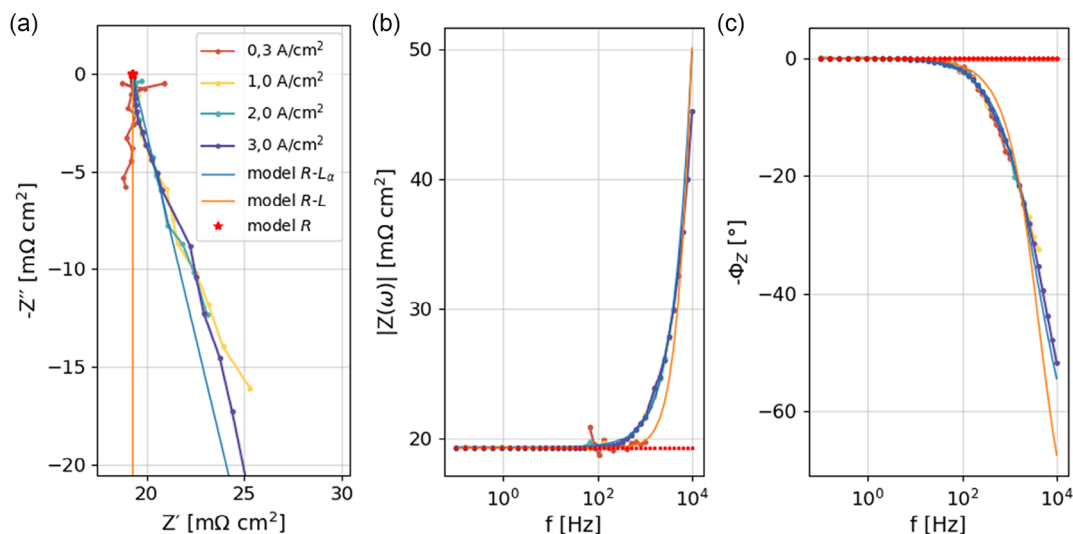


Figure 3. a) Nyquist, b) Bode magnitude, and c) Bode phase plots of short-circuit measurements at different current densities, and of the $R-L_\alpha$, $R-L$, and R fitting models.

However, the setup consists of a potentiostat connected to the test cell via a power supply with prolonged cables and this can create a mutual inductance between cables over multiple ways and electrical contacts.^[36] Cables twisting is considered to decrease their yield to the stray impedance,^[1] but even a small straight piece of wire can present some self-inductance.^[4] In addition, the electrical coupling of the cell to the cables is achieved via 2- and not 4-points connection, which has been seen to create a lead inductance and resistance.^[9]

Since these parasitic effects could not be avoided, an ECM has to be used to assess them. There are a different ways to model the inductive stray impedance: 1) a simple pure inductance (in Figure 3 model $R-L$),^[31] 2) pure inductance in parallel with a resistance,^[13,37] and 3) a modified inductance (in Figure 3 model

$R-L_\alpha$).^[35,38] After assessing all the mentioned models, the one, which describes the results with the highest accuracy, which means least χ^2 , is a modified inductive reactance (L_α) in series to a resistance (R_{ohm}), see the ECM in Figure 2. The different fitting models are shown in Figure 3.

ECM results acquired in SC measurement are shown in Figure 4. Figure 4a shows constant values of α and L for all the current densities apart from increased values at 0.3 A cm^{-2} . The latter is assigned to the specifications of the potentiostat and its lower accuracy at lower current densities and to the many noisy points discarded in data processing. The difference between low (0.3 A cm^{-2}) and medium high (1 A cm^{-2}) current densities EIS response before filtering of the data points is evident in Figure 4b,c. At 0.3 A cm^{-2} , the

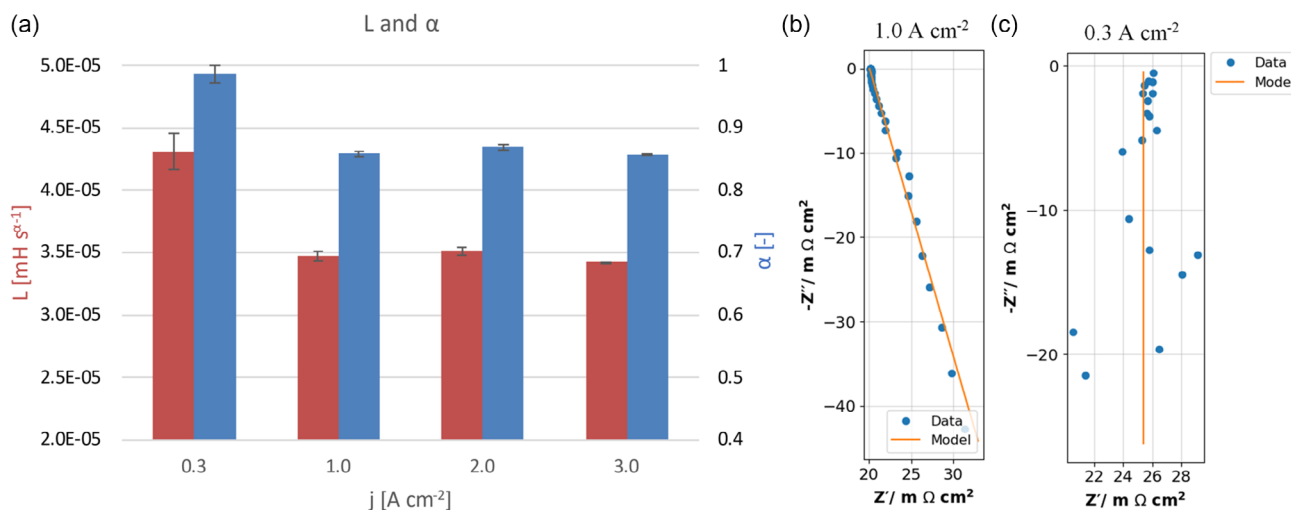


Figure 4. a) Average values of L and α of the modified inductive reactance at different current densities; electrochemical impedance spectroscopy (EIS) spectra at b) 1 A cm^{-2} and c) 0.3 A cm^{-2} during short-circuit (SC) measurements (blue points) and the respective results of fitting of the $R-L_\alpha$ model (orange lines).

scattered and noisy curve, must be reduced to fewer and less noisy points, which leads to a different fitting result than the undisturbed EIS at 1 A cm^{-2} and higher current densities. As the analysis for 0.3 A cm^{-2} is hence based on less points, a higher discrepancy and lower reliability needs to be taken into account. For current densities of 1 A cm^{-2} and higher, the results are consistent and no longer depend on the used current density, as expected for an inductance resulting from an unaltered setup arrangement and cable positions. The SC measurement can, therefore, be used to show external effects to the MEA. The resulting inductive characteristic is assessed via an ECM, which provided the values for the ECM evaluation of in situ EIS.

3.2. ECM Fitting of In Situ EIS Measurements

The EIS of in situ measurement are shown in **Figure 5**. It is evident how the spectrum impedance reduces with current density, while the intercept with the x-axis increases with current density. This phenomenon is caused by a decreased water temperature introduced into the anode and cathode inlets at increasing current densities. This occurs because the system temperature is defined by the anode outlet and at higher current densities, the water at the outlet is warmer due to the heat released by the reaction. As consequence, the thermal management reduces the temperature of the system and the water flushed into the cell is colder. This effect results in a shift of the entire EIS spectrum to higher impedance. This is, however, not the focus of this paper and must be proven within a targeted study.

Similarly to the SC measurements, the EIS performed during in situ measurements show an inductive behavior at all current densities, but only at frequencies above 450 Hz. This is a result of the competing effects at frequencies between 60 and 450 Hz: the impedance caused by the CCM is almost one order of magnitude higher than the SC, and therefore the influence of parasitic effect on the inductance shifts to higher frequencies.

After an initial successful evaluation on the validity of the data via KKT, the EIS spectrum is fitted via the mentioned ECM (see Figure 1). In situ measurements tend to fit two times faster and

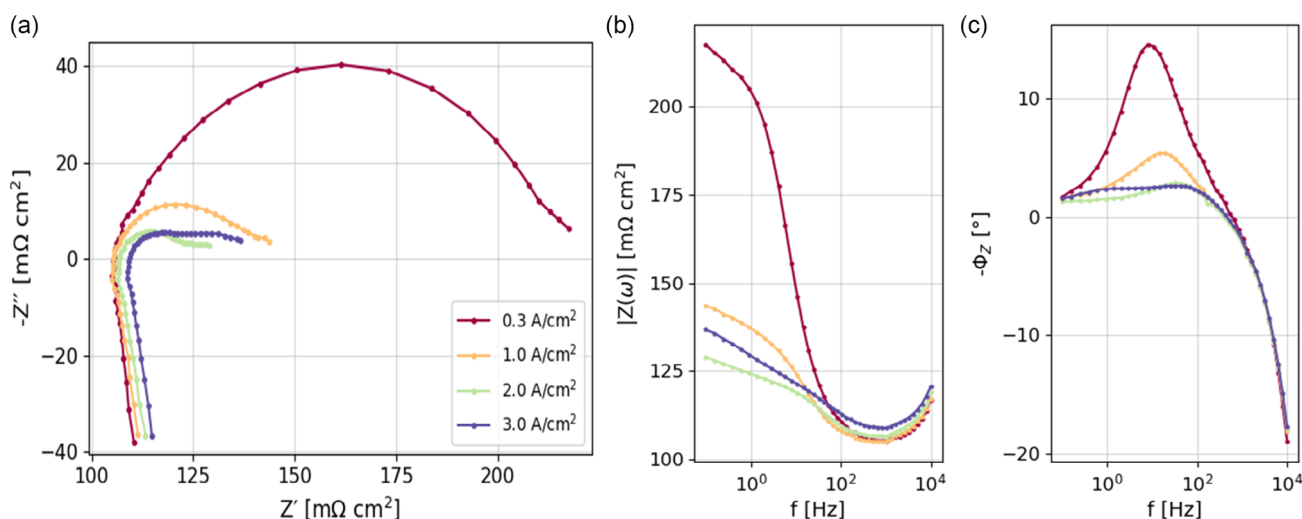


Figure 5. a) Nyquist, b) Bode magnitude, and c) Bode phase plots of in situ measurements at different current densities.

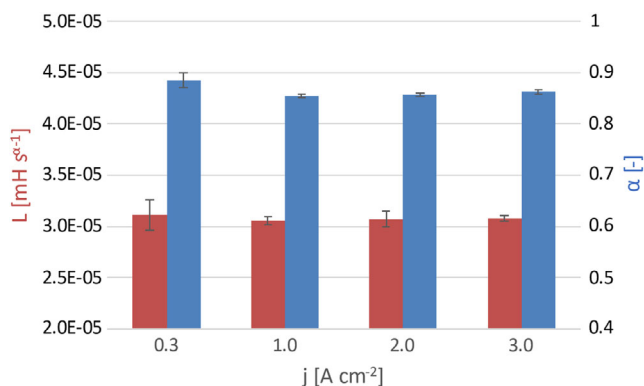


Figure 6. Average values of L and α from the ECM of EIS at different current densities in in situ measurements.

with up to an 80% lower χ^2 with initial values based on the L_{α} from the modeling of the SC measurement. Therefore, the initial evaluation of the inductance through SC improves the ECM evaluation of in situ spectra.

In case the initial values of the inductance are the ones from SC, but they are left free to fit according to the evaluating algorithm, the L and α parameters show similar trends and values as in SC (compare **Figure 4** and **6**). The values remain constant for all current densities, just the inductivity is in average $0.5 \times 10^{-5} \text{ mH s}^{-1}$ lower than in SC. This difference could be caused by the reduced data in SC, and by the high degree of freedom in fitting ECM.

When an inductance is present, the shape of the EIS spectrum is modified and precludes to recognizing some effects, for example, an R - C arc. The underlying effects are partially covered by the inductance and may not appear in the EIS spectrum, or they could show different values because of the inductance.^[9,20] An impact of these effects is shown in **Figure 7**, where modifications of a spectrum with α and L changes are presented. At increasing L and decreasing α , the high-frequency region is distorted and the HFR shifts to higher values.

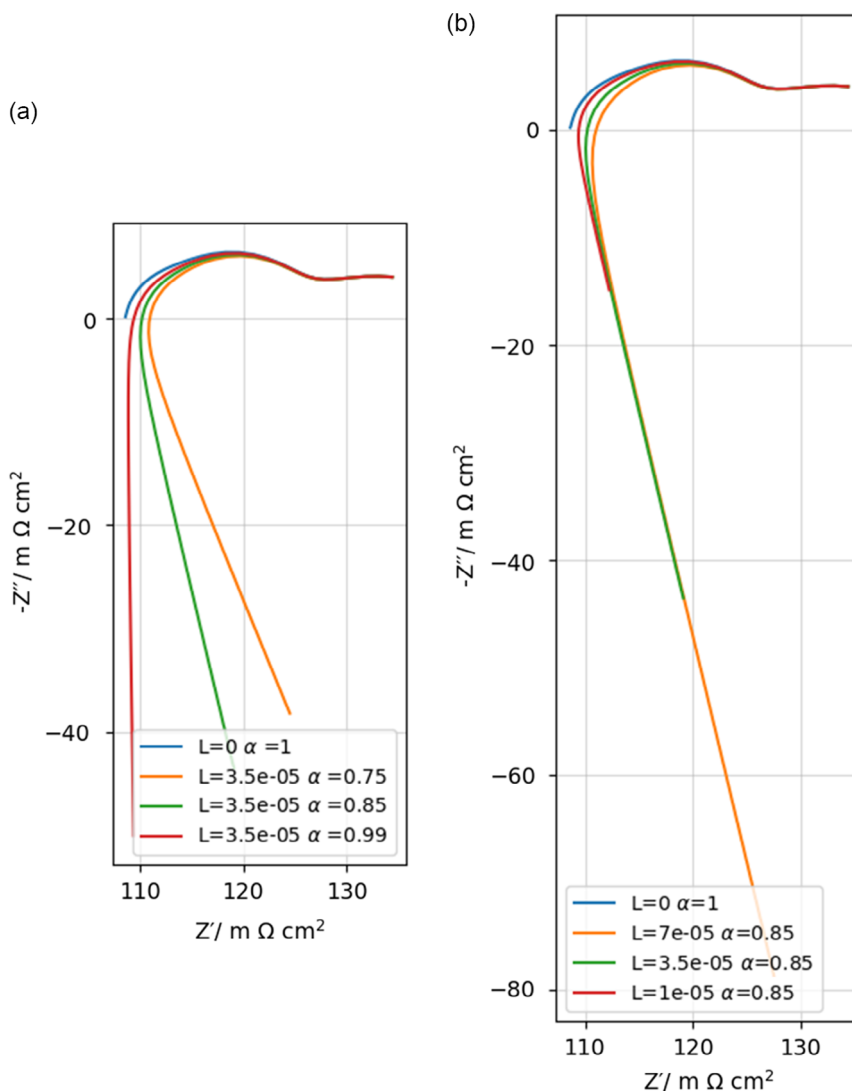


Figure 7. Influence of the variation of a) α and b) L on the shape of a Nyquist plot for EIS spectra.

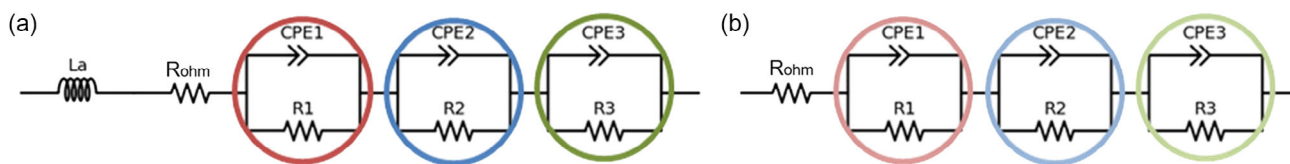


Figure 8. ECM a) including and b) not including a modified inductance.

The influence of the inductance on the spectra was evaluated by comparing the results from two different ECM (**Figure 8**): with and without the inductive points in EIS and inductive element in ECM (**Figure 9**). In the former case, the raw data were simply fitted according to the model in **Figure 8a**. While, in the latter case, the inductive part of the data were excluded (no points below x-axis), so that only the portion of data with capacitive characteristic is analyzed by the model in **Figure 8b**. This second approach agrees with the typical discarding of inductive points during many studies on PEM water electrolysis cells.^[6,11,39–41]

Both models in **Figure 8** present an R_{ohm} and three $R//CPE$ groups, which model effects at high (red, Z_{HF}), middle (green, Z_{mF}), and low (blue, Z_{LF}) frequencies.

The results of the two models are shown in **Figure 9** for an EIS at 3 A cm^{-2} . The arcs representing the results of the three $R//CPE$ are plotted for both cases with origin in the R_{ohm} resulting from the fitting. The ECM result follows the raw data better when the inductance is included, and the $R//CPE$ arcs are not matching in the two cases (**Figure 9** above compared to below).

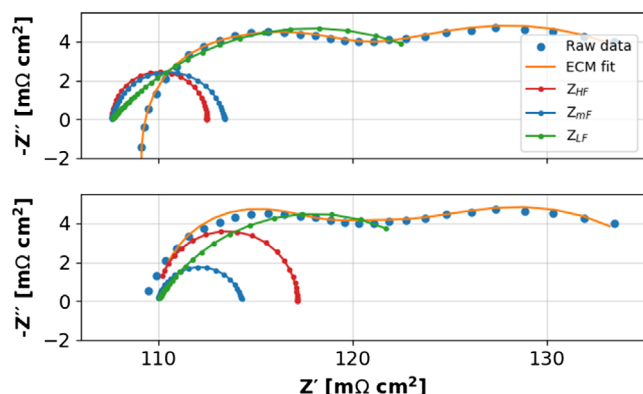


Figure 9. Raw data and ECM fitting results including (figure above) and not including (figure below) the inductance at 3 A cm^{-2} . Resistance in parallel with a constant phase element (R//CPE) arcs at high (red), middle (blue), and low (green) frequencies are plotted starting from R_{ohm} value.

The ECM results also exhibit a different R_{ohm} value. In case the inductive points are excluded, the R_{ohm} is very similar to the EIS intercept with the x-axis in the Nyquist plot, the so-called HFR. When the inductance is included, the R_{ohm} is smaller than the HFR,^[42] as was predicted from Figure 7. The shift of the evaluated R_{ohm} is present at all current densities. Similar evidence was also quantified and modeled by Shin and Cruz-Manzo for SOC electrolysis cells and fuel cells, respectively.^[4,13] The higher the L is, the larger the shift of R_{ohm} will be, and the same with a lower α .

Detailed mechanisms, like restrictions at the triple-phase boundary at the catalyst layer due to proton or electron movements, or limitations related to gas bubble formations, or reaction kinetics are the processes described by the above R//CPE elements.^[8,31,43] These mechanisms can be attributed to anode and cathode electrodes, but it is widely accepted that the anode contributes to most of the losses.^[28,44]

The charge-transfer resistance of faradaic processes is expected to decrease with increasing current densities and the double-layer capacitance of the anode reaction was seen to also decrease with current density via reference electrode analysis by Sorsa et al.^[45–47] This means that their peak frequency is expected to increase with increasing current densities.

Recently the peak frequencies (or characteristic frequencies) were proposed to identify and characterize the processes occurring in electrochemical devices including water electrolysis MEA.^[37,45,48] Peak-frequency analysis was, therefore, evaluated in case of inclusion (darker color) or not (lighter color) of the inductance and plotted for each R//CPE group in **Figure 10**. It is evident that the two approaches never provide corresponding results. In case of inclusion of the inductance, the peak frequencies increase with current density for mF and HF R//CPE, which correspond to the tendency of faradaic processes. While no clear trend is visible in case the inductance is excluded from the ECM analysis.

The fitting without inductance consideration leads to high discrepancy of peak-frequency values and shifts the HF and LF R//CPE to lower values, which is likely caused by the exclusion of points at high frequencies. It must be remembered that

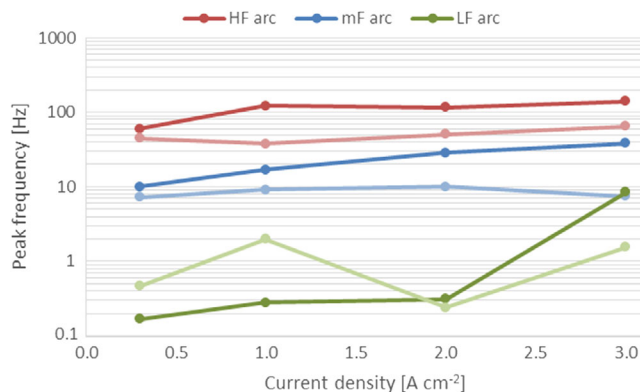


Figure 10. Peak frequencies of the R//CPE groups at high (HF in red), middle (mF in blue), and low (LF in green) frequencies for ECM with (darker color) and without (lighter color) inductance at $0.3, 1, 2,$ and 3 A cm^{-2} .

parasitic effects are present even at frequencies where the EIS follows a capacitive behavior. Hence, their effects are evaluated from the model without inductance as R//CPE groups, which leads to misinterpretation of the results.

Since the LF R//CPE appears in Bode plot just at 3.0 A cm^{-2} (Figure 5), mass transport limitations are supposed to be associated to its behavior. The peak-frequency trend for the ECM without inductance does not follow any trend, scattering illogically at increasing current density. With the inductance inclusion, in contrast, the peak frequency looks stable at low current densities, as it is supposed to be when no changes in mass transport limitation appear, up 3 A cm^{-2} . At this current density, the EIS spectra show an additional arc, which can increase the peak frequency of this R//CPE group due to the increased charge-transfer resistance describing the diffusion limitations of gas bubbles.

4. Conclusion

EIS is a widely used method to evaluate the internal effects in electrochemical technologies, such as electrolysis cells. However, influences external to the object of study can also contribute to the measured EIS spectra in form of so-called parasitic effects. They often result in an inductance at high frequencies of the spectrum. When these parasitic effects cannot be avoided, the common approach in literature is to simply exclude the inductive points (below the x-axis in Nyquist plot) from the EIS analysis. This study demonstrates that this procedure can lead to incorrect results and presents a method how to better evaluate EIS spectra in case inductance is present at high frequencies.

The first part assesses if the measured inductive effects are caused by the external setup (electrical setup, cables, connectors, and cell housing) or by the object of study (CCM). This was evaluated via a SC measurement using the same setup and the identical test cell as in in situ measurements, but in which the CCM is replaced with a simple conductor without capacitive, inductive, or resistive contribution to the EIS spectrum. The resulting EIS spectrum was used to quantify the parasitic effects, by fitting the EIS spectra to a modified inductance in series to a resistance.

Results show that parasitic effects are becoming significant at frequencies higher than 60 Hz, and they are independent from the applied current density. This proves that in our case the effects are a characteristic property of the external setup and not of the CCM.

After assessing the external effects, it is important to include them in an ECM, and not to cut the EIS curve at the x-axis and evaluate those reduced points with an ECM. Inductive artifacts mask the cell's electrochemical behavior and lead to incorrect interpretation of the EIS high-frequency region. In particular, this inductance can increase the Ohmic resistance, calculated as the intersection with the x-axis (HFR). In addition, these parasitic effects influence the distribution of the electrochemical effects evaluated as R//CPE elements, which are attributed to the CCM. If no inductance is included in the evaluation, the electrochemical effects shift to lower characteristic frequencies, and they can lead to misinterpretation of trends dependent on the current densities. The results of this study can be generalized to any EIS with an inductance because any parasitic response in an EIS competes with effects that are evolving inside the cell at many frequency points.

Acknowledgements

The author would like to thank Fraunhofer Cluster of Excellence "Integrated Energy System" for financial support and the electrolysis group at Fraunhofer ISE for any technical assistance and Dietmar Gerteisen from the fuel cell department for the fruitful discussion, which allowed them to fulfill this study. A.P. acknowledges the Department of Science and Innovation (DSI), South Africa, for the financial support via HySA Centre of Competence KP5 program. The views expressed in the article do not necessarily represent the views of the DOE or the U.S. Government.

Open Access funding enabled and organized by Projekt DEAL.

Conflict of Interest

The authors declare no conflict of interest.

Data Availability Statement

The data that support the findings of this study are available from the corresponding author upon reasonable request.

Keywords

electrochemical impedance spectroscopy (EIS), equivalent circuit model (ECM), high-frequency resistance (HFR), inductance, parasitic effects, proton exchange membrane (PEM) water electrolysis

Received: April 5, 2023

Revised: May 15, 2023

Published online: June 20, 2023

[1] S. Wang, J. Zhang, O. Gharbi, V. Vivier, M. Gao, M. E. Orazem, *Nat. Rev. Methods Primers* **2021**, 1, 41.

[2] D. A. Harrington, P. van den Driessche, *Electrochim. Acta* **2011**, 56, 8005.

- [3] N. Meddings, M. Heinrich, F. Overney, J.-S. Lee, V. Ruiz, E. Napolitano, S. Seitz, G. Hinds, R. Raccichini, M. Gaberšček et al., *J. Power Sources* **2020**, 480, 228742.
- [4] S. Cruz-Manzo, R. Chen, P. Rama, *J. Fuel Cell Sci. Technol.* **2012**, 9.
- [5] J. van der Merwe, K. Uren, G. van Schoor, D. Bessarabov in *IEEE Int. Conf. on Industrial Technology (ICIT)*, IEEE, Piscataway, NJ **2013**, pp. 668–672.
- [6] S. Siracusano, S. Trocino, N. Briguglio, V. Baglio, A. S. Aricò, *Mater.* **2018**, 11.
- [7] N. Cogger, N. Evans, *Contribution from Solartron Analytical* **1999**.
- [8] K. Elsoe, L. Grahl-Madsen, G. G. Scherer, J. Hjelm, M. B. Mogensen, *J. Electrochem. Soc.* **2017**, 164, F1419.
- [9] B. Savova-Stoynov, Z. B. Stoynov, *J. Appl. Electrochem.* **1987**, 17, 1150.
- [10] H. Göhr, M. Mirnik, C. Schiller, *J. Electroanal. Chem. Interfacial Electrochem.* **1984**, 180, 273.
- [11] M. Suermann, B. Bensmann, R. Hanke-Rauschenbach, *J. Electrochem. Soc.* **2019**, 166, F645.
- [12] M. Suermann, A. Pătru, T. J. Schmidt, F. N. Büchi, *Int. J. Hydrog. Energy* **2017**, 42, 12076.
- [13] E.-C. Shin, P.-A. Ahn, H.-H. Seo, J.-M. Jo, S.-D. Kim, S.-K. Woo, J. H. Yu, J. Mizusaki, J.-S. Lee, *Solid State Ion.* **2013**, 232, 80.
- [14] R. Makharia, M. F. Mathias, D. R. Baker, *J. Electrochem. Soc.* **2005**, 152, A970.
- [15] S. Cruz-Manzo, *JEPT* **2020**, 2, 1.
- [16] D. Klotz, A. Weber, E. Ivers-Tiffée, *Electrochim. Acta* **2017**, 227, 110.
- [17] C. Erinmwingbovo, F. La Mantia, *Sci. Rep.* **2021**, 11, 1362.
- [18] N. Fouquet, C. Doulet, C. Nouillant, G. Dauphin-Tanguy, B. Ould-Bouamama, *J. Power Sources* **2006**, 159, 905.
- [19] S. Asghari, A. Mokmeli, M. Samavati, *Int. J. Hydrog. Energy* **2010**, 35, 9283.
- [20] E. Barsoukov, J. R. Macdonald, in *Impedance Spectroscopy. Theory, Experiment, And Applications*, Wiley-Interscience, Hoboken NJ **2005**.
- [21] S. H. Frensch, A. C. Olesen, S. S. Araya, S. K. Kær, *Electrochim. Acta* **2018**, 263, 228.
- [22] J. Rodríguez, S. Palmas, M. Sánchez-Molina, E. Amores, L. Mais, R. Campana, *Membranes* **2019**, 9, 129.
- [23] G. Raikova, P. Carpanese, Z. Stoynov, D. Vladikova, M. Viviani, A. Barbucci, *Bulg. Chem. Commun.* **2009**, 41, 199.
- [24] S. Rau, Dissertation, Universität Stuttgart, **2014**.
- [25] A. Papaderakis, D. Tsiplakides, S. Balomenou, S. Sotiropoulos, *J. Electroanal. Chem.* **2015**, 757, 216.
- [26] R. Alink, M. Schüßler, M. Pospischil, D. Erath, D. Gerteisen, *J. Power Sources* **2016**, 327, 526.
- [27] L. Zhao, H. Dai, F. Pei, P. Ming, X. Wei, J. Zhou., *Energies* **2022**, 15, 386
- [28] C. Rozain, P. Millet, *Electrochim. Acta* **2014**, 131, 160.
- [29] C. Rozain, E. Mayousse, N. Guillet, P. Millet, *Appl. Catal. B: Environ.* **2016**, 182, 123.
- [30] E. Rasten, G. Hagen, R. Tunold, *Electrochim. Acta* **2003**, 48, 3945.
- [31] P. Lettenmeier, S. Kolb, F. Burggraf, A. S. Gago, K. A. Friedrich, *J. Power Sources* **2016**, 311, 153.
- [32] K. Elsoe, M. R. Kraglund, L. Grahl-Madsen, G. G. Scherer, J. Hjelm, S. H. Jensen, T. Jacobsen, M. B. Mogensen, *Fuel Cells* **2018**, 18, 640.
- [33] I. Dedigama, P. Angeli, K. Ayers, J. B. Robinson, P. R. Shearing, D. Tsaoulidis, D. Brett, *Int. J. Hydrogen Energy* **2014**, 39, 4468.
- [34] C. H. Hsu, F. Mansfeld, *Corrosion* **2001**, 57, 747.
- [35] M. Murbach, B. Gerwe, N. Dawson-Elli, L. Tsui, *JOSS* **2020**, 5, 2349.
- [36] B. W. Veal, P. M. Baldo, A. P. Paulikas, J. A. Eastman, *J. Electrochem. Soc.* **2014**, 162, H47.
- [37] I. V. Pushkareva, M. A. Solovyev, S. I. Butrim, M. V. Kozlova, D. A. Simkin, A. S. Pushkarev, *Membranes* **2023**, 13, 192.

- [38] N. Murer, The Modified Inductance Element La Bio-Logic EC – Lab. Application. Note, **2012**.
- [39] Z. Kang, M. Wang, Y. Yang, H. Wang, Y. Liu, J. Mo, J. Li, P. Deng, C. Jia, X. Tian, *Int. J. Hydrog. Energy* **2022**, *47*, 5807.
- [40] M. Suermann, T. Gimpel, L. V. Böhre, W. Schade, B. Bensmann, R. Hanke-Rauschenbach, *J. Mater. Chem. A* **2020**, *8*, 4898.
- [41] C. Rakousky, U. Reimer, K. Wippermann, M. Carmo, W. Lueke, D. Stolten, *J. Power Sources* **2016**, *326*, 120.
- [42] I. Franzetti, A.-L. Chan, A. Pushkarev, S. Metz, *Proc. of WHEC-2022, 23rd World Hydrogen Energy Conf.*, **2022**, p. 391.
- [43] J. Fleig, J. Maier, *J. Electrochem. Soc.* **1997**, *144*, L302.
- [44] Z. Kang, S. M. Alia, J. L. Young, G. Bender, *Electrochim. Acta* **2020**, *354*, 136641.
- [45] A. S. Pushkarev, I. V. Pushkareva, S. P. du Preez, D. G. Bessarabov, *Catalysts* **2023**, *13*, 554.
- [46] O. Sorsa, J. Nieminen, P. Kauranen, T. Kallio, *J. Electrochem. Soc.* **2019**, *166*, F1326.
- [47] P. Millet in *PEM Electrolysis for Hydrogen Production: Principles and Applications*, **2016**, pp. 179–217.
- [48] Y. Li, Y. Jiang, J. Dang, X. Deng, B. Liu, J. Ma, F. Yang, M. Ouyang, X. Shen, *Chem. Eng. J.* **2023**, *451*, 138327.